

Negative afterimages facilitate the detection of real images

Frederick A. A. Kingdom, Samir Touma and Ben J. Jennings*

McGill Vision Research, Department of Ophthalmology and Vision Sciences, Montreal General Hospital, 1650 Cedar Ave., Rm L11.112, Montreal, Quebec, H3G 1A4, Canada

* Centre for Cognitive Neuroscience, College of Health, Medicine and life Sciences, Brunel University London, U.K.

Abstract

Negative, or complementary afterimages are experienced following brief adaptation to chromatic or achromatic, i.e. “colored” stimuli, and are believed to be formed in the post-receptoral layers of the retinae. Afterimages can be cancelled by the addition of real images, suggesting that afterimages and real images are processed by similar mechanisms. However given their retinal origin, afterimage signals represented at the cortical level might have different spatio-temporal properties from their real images counterparts. To test this we determined whether afterimages reduce the contrast threshold of added real images, i.e. produced the classic “dipper” function characteristic of contrast discrimination, a behavior believed to be cortically mediated. Stimuli were chromatic and achromatic disks on a grey background. Observers adapted for 1.5 secs to two side-by-side disks of a particular color. Following stimulus offset, a test disk added to one side was ramped downwards for 1.5 seconds to approximately match the temporal characteristic of the afterimage, and the observer was required to indicate the side containing the test disk. The test hue was either the same as that of the afterimage or a different hue. The independent variable was the contrast of the adaptor. Dippers followed by masking functions were observed in most conditions

in which the afterimage and test colors had the same hue or brightness. We conclude that afterimages are represented similarly to their real image counterparts at the cortical level.

Introduction

Fixating a chromatic (e.g. red or green) or achromatic (e.g. black or white) surface for a few seconds generates a complementary afterimage on a subsequently viewed neutral grey surface. The afterimage exponentially diminishes in strength over time, usually in a matter of seconds. Chromatic and achromatic afterimages are believed to originate in the retina (Zaidi et al., 2012), initially via a reduction in cone receptor sensitivity from stimulation by a strong light, followed by opponent-channel processing beginning in the post-receptoral layers. Although it has been shown that the hues of color afterimages are not exactly complementary to those of the images that produce them (Livitz et al., 2015), their *near*-complementarity is consistent with their being generated by the red-green, blue-yellow and black-white mechanisms of classical opponent-color theory (Hering, 1920/1964), and/or the opponent mechanisms of the cardinal-axis color space (Krauskopf, Williams & Heeley, 1982).

Most evidence suggests that afterimages are transduced by similar mechanisms to those that signal their real image counterparts. For example, color afterimages can be cancelled by the addition of real images (Anstis, Rogers & Henry, 1978; Zaidi et al., 2012) and afterimages raise the contrast thresholds of real images that are added to them (Kelly & Martinez-Uriegas, 1993). Moreover, the effect of luminance contours on color appearance is similar for both afterimage colors and real colors (Van Lier, Vergeer & Anstis, 2009; Anstis, Vergeer & Van Lier, 2012). Consistent with the idea of a common mechanism for real images and afterimages, Schwartz, Hsu & Dayan (2007) argue that by-and-large we are unaware of our state of adaptation, so although in popular demonstrations and laboratory investigations observers may be aware that they are experiencing an afterimage, in every-day vision this may not be so. In keeping with Schwartz et al. (2007), Webster (personal communication) argues that afterimages should perhaps not be considered as “illusory” at all, but rather as “real” images in a different state of adaptation. While bearing this argument in mind, the present study nevertheless maintains for ease of exposition the distinction between an afterimage and a real image.

Although afterimages are produced in the retina (Zaidi et al., 2012) there is evidence that the cortex may be involved in their modification (Dong, Holm & Bao, 2017; Zaidi et al., 2012). For example, the strength of an afterimage is dependent to some extent on attention, that is, it is weaker

if the inducer is attended to during the adaptation phase (Suzuki & Grabowecky, 2003). There may therefore be significant differences in the spatio-temporal properties of afterimages and real images when represented at the cortical level. Powell et al. (2012) found that high frequency edges defined by luminance contrast increased afterimage strength to a greater extent than a physical stimulus of equal appearance and concluded that color afterimages are therefore “special”. Although this does not necessarily imply that the mechanisms that signal real images and afterimages are fundamentally different, it does suggest there are differences at the cortical stages of visual processing where luminance and color contrast interact.

In this communication we consider to what extent afterimages and real images are similar in terms of their ability to mediate contrast discrimination behavior. The threshold-versus-contrast, or TvC function describes how contrast discrimination thresholds vary as a function of baseline, or “pedestal” contrast. One typically finds that in the region of pedestal contrasts at or near their own detection threshold, test increment thresholds are lower compared to those obtained in the absence of a pedestal. This region is commonly termed the “dipper” but referred to here also as the region of “facilitation”. At higher pedestal contrasts discrimination thresholds rise above the no-pedestal thresholds, a region termed here “masking”. Although the precise reason for the dipper is disputed (Solomon, 2009), a dipper followed by masking is generally believed to be a signature that the test increment and pedestal are processed in a similar way. The selectivity of the TvC function to spatial-frequency (Legge & Foley, 1980) and orientation (Ross & Speed, 1991) suggests that contrast discrimination is mediated at the cortical level. Kelly & Martinez-Uriegas (1993) found that chromatic afterimages raise the thresholds of real increments added to them. Here we ask whether an afterimage not only masks an added real image, but also facilitates its detection when at subthreshold levels. If it does this would suggest that at the cortical level afterimages are represented similarly to real images, including at sub-threshold levels, at least when mediating contrast discrimination behavior.

In general, the effect of adaptation on the TvC function is to increase thresholds across the entire pedestal range (Ross & Speed, 1991; Webster, 1996; Ross, Speed & Morgan, 1993), though there is evidence that under certain conditions and for certain observers contrast thresholds can be lowered by adaptation (Greenlee & Heitger, 1988; Abbonizio, Langley & Clifford, 2002). Using afterimages as pedestals invites the possibility that, at least for stimuli processed by opponent mechanisms, adaptation might produce substantial and consistent reductions in contrast thresholds. In light of this possibility it is worth emphasizing the difference between the

conventional protocol for testing the effect of adaptation on the TvC function and that used here. In the conventional protocol, there are three physically distinct stimuli: adaptor, mask and test. On each trial following adaptation, the mask and test are presented together in one alternative and the mask alone in the other, and the observer is required to indicate the alternative containing the test. With the afterimage protocol used here, illustrated in Fig. 2, there are only two physically distinct stimuli: adaptor and test. After adaptation the two alternatives are with-test and without-test, and the observer is required to identify the with-test alternative. The “mask” in this situation is the afterimage.

To summarise: the aim of this communication is to determine whether afterimages, like real images, facilitate the detection of added real images that are matched in hue or brightness. In doing so we will determine to what extent afterimages and real images are represented similarly, in particular at sub-threshold levels, in the cortex.

Methods

Observers

Five observers participated in the experiments. Three were authors, though one author was naïve as to the purpose of the main experiment when tested. The remaining two observers were volunteers who were naïve as to the purpose of the experiments. All observers had 6/6 visual acuity and tested normal on the Ishihara color deficiency test (24 plates edition). All observers completed the achromatic afterimage experiment, and all but one observer the chromatic afterimage experiment. Two observers completed the additional experiment with the red test images. All experiments were conducted in accordance with the Declaration of Helsinki and the Research Institute of the McGill University Health Centre (RI-MUHC) Ethics Board. Observer initials on graphs have been anonymized in accordance with requirements of the RI-MUHC Ethics Board.

Equipment

Stimuli were generated by a VISAGE graphics card (Cambridge Research Systems, Riverside, Kent, UK) and displayed on a Sony Trinitron F500 flat-screen monitor. The R (red), G (green) and B (blue) gun outputs of the monitor were gamma-corrected after calibration with an Optical

photometer (Cambridge Research Systems). The spectral emission functions of the R, G and B phosphors were measured using a PR 640 spectral radiometer (Photo Research, Syracuse, NY, USA), with the monitor screen filled with red, green, or blue at maximum luminance. The CIE coordinates of the monitor phosphors were R: $x = 0.624, y = 0.341$; G: $x = 0.293, y = 0.609$; B: $x = 0.148, y = 0.075$. Viewing distance to the monitor was 100cm.

Color space

Example stimuli are illustrated in Figs. 1 and 2. They were circular patches defined by directions within the DKL color space (Derrington, Krauskopf, & Lennie, 1984). The DKL consists of two cardinal axes defined by combinations of long-wavelength-sensitive (L), middle-wavelength-sensitive (M), and short-wavelength-sensitive (S) cone *contrasts*. The three cone contrasts are defined as: $L_c = \Delta L/L_b$, $M_c = \Delta M/M_b$ and $S_c = \Delta S/S_b$. The denominator in each cone-contrast term refers to the cone excitation of the background, which was a mid-grey color with CIE chromaticity $x = 0.282$ and $y = 0.311$, and luminance 40 cd/m^2 . The numerator in each cone contrast term represents the difference in cone excitation between the disk and background. The chromatic axes of the DKL space are $L-M$ and $S-(L+M)$, which correspond to color directions red-cyan and violet-lime, with chromatic contrast given by the length of the vector along the axis. The luminance axis is defined as $L+M$ and corresponds to the black-white direction. The R (red), G (green) and B (blue) display-monitor values of points within the DKL space were selected by means of a 3×3 conversion matrix derived by multiplication of the spectral power distributions of the display's R, G and B phosphors (as measured with a SpectroCAL from Cambridge Research Systems), and the human $L-, M-$ and $S-$ cone fundamentals (Smith & Pokorny, 1975), as described for example in Brainard & Stockman (2010).

The DKL space is a cardinal color space in that the colors uniquely stimulate the three post-receptoral mechanisms. The relative cone contrast inputs to these mechanisms have been estimated to be as follows: kL_c+M_c for the luminance (LUM) mechanism, producing black and white; L_c-M_c for the mechanism that differences L and M cone-contrasts, producing red and cyan; $S_c-(L_c+M_c)/2$, or simply the “ S ” mechanism that differences the S from the sum of L and M cone-contrasts, producing violet and lime (Cole, Hine & McIlhagga, 1993; Sankeralli & Mullen, 1996; Stromeyer, Cole & Kronauer, 1985). The parameter k determines the relative weights of the L and M cone-contrast inputs to the luminance mechanism, and since this value varies between observers it was established separately for each subject (see below). In order to *isolate* the three cardinal mechanisms the stimuli must be constructed from cone inputs such that the $L-M$ stimulus does not activate either the LUM or the S mechanism, the S stimulus neither the LUM nor $L-M$ mechanism,

and the *LUM* stimulus neither the *S* nor *L-M* mechanism. Kingdom, Rangwala and Hammamji (2005) used the following combinations of L_c , M_c and S_c to achieve this:

$$'L-M' = L_c - kM_c + S_c(1-k)/2 \quad \text{Eq. 1a}$$

$$'S' = S_c \quad \text{Eq. 1b}$$

$$'LUM' = L_c + M_c + S_c \quad \text{Eq. 1c}$$

The measures of contrast were calculated as follows: for *L-M*, the difference between L_c and M_c ; for *S*, simply S_c ; for '*LUM*' the contrast assigned to each cone, e.g. L_c .

Stimulus colors

The chromatic disks employed were violet, lime and red. The violet and lime colors lay at the positive and negative poles of the *S* cone axis, whereas the red color lies at the positive pole of the *L-M* axis. The achromatic disks were white and black and lay at the positive and negative poles of the luminance axis. We investigated lime chromatic afterimages, produced by adaptation to violet, and dark grey afterimages, produced by adaptation to white. In the main experiment the test images were therefore also lime and dark grey respectively. An additional experiment used the same violet adaptor and lime afterimage, but with a red test image.

The disks were surrounded by a 1-pixel wide black circle that was present throughout each experimental session. It served two purposes. First it helped constrain any spreading of the isoluminant colors (Feitosa-Santana, D'Antona, & Shevell, 2011), and second it eliminated any positional uncertainty as to where they were, such that any dipper function observed in the data could not be attributed to a reduction in positional uncertainty as the pedestals became visible.

Procedure

In what follows we describe the 5 step procedure employed in the experiments.

Step 1: Measurement of isoluminance

Because of inter-observer variation in the relative weightings of the *L* and *M* cones that feed the luminance mechanism, it was necessary to ensure that the *L-M* cone modulations were isoluminant. We used the criterion of minimum perceived motion. A 0.05 contrast, 0.5 cpd *L-M* (red-cyan) sinusoidal grating was set to drift at about 1.0 Hz. Observers pressed a key to add or

subtract luminance ($L+M$) contrast to the grating until they perceived motion at a minimum. Each observer made between 20 and 30 settings. The average amount of luminance contrast added (or subtracted) is given for each observer in Table 1 of the Appendix. Although S cones only contribute to the luminance mechanisms under extreme conditions (Eskew, McLellan, & Giulianini, 1999; Ripamonti et al., 2009), there is always the possibility of calibration error with S stimuli, so for each observer we also measured the isoluminant point for a drifting 0.25 contrast S (violet-lime) grating with the same spatiotemporal parameters as that used for the $L-M$ stimulus. The ratios of $L+M$ to S contrast needed to make the S stimuli isoluminant are also given in Table A1.

Step 2: Cardinal axis contrast matching

We next equated the perceived contrasts of the colors along the two cardinal axes of the DKL color space. We did this so that perceived contrast would remain approximately constant when in Step 3 (below) observers adjusted the color direction of a real image to match that of the afterimage. The procedure we employed is illustrated in Fig. 1a. The violet-lime pair was fixed at a contrast of 0.22 and alternated in time with the adjustable red-cyan pair (both 1 sec with raised cosine envelopes). During the alternation observers used a key press to either increase or decrease the contrast of the red-cyan pair until they perceived the contrasts of the two pairs to be equal at which point they pressed a button to register their response. They made 10 settings and the mean of the settings was calculated and shown in Table A1. This mean was divided by 0.22 (the fixed violet-lime contrast) to give the red-cyan/violet-lime contrast ratio r used in the following step.

Step 3: Hue matching of afterimages with real images

To obtain colors matched in hue to the lime afterimage a combined hue and contrast matching method was employed, as illustrated in Fig. 1b, using the same temporal sequence of adaptor and test as in the main experiment illustrated in Fig 2b. A violet adaptor on one side of fixation repeatedly alternated in time with an adjustable test stimulus on the other side of fixation. The task for the subject was to adjust, using two sets of keys, both the color direction θ (in the DKL color space) and the color contrast or saturation C , (the vector length of θ), until it matched the hue and contrast of the afterimage. During the adjustment of θ at a given C the red-cyan and violet-lime contrasts were set to $C r \sin(\theta)$ and $C \cos(\theta)$ respectively (r being determined by Step 2), thus keeping the perceived contrast of the mixture constant making the adjustment of θ easier. When the observer was satisfied with the match he/she pressed a key and the response was recorded. 10 adjustments were made and the average values calculated. The hue matches for all observers are given in Table A1

(A=Appendix) and were close to or at a θ of 180 deg, i.e. complementary to the $\theta = 0$ deg violet adaptor.

Step 4: Contrast matching of afterimages with real images

In order to equate the perceived contrasts of the afterimages with the perceived contrasts of the real image pedestals used in the main experiments (Steps 5 and 6) observers used the matching procedure illustrated in Fig. 1b, this time for a range of adaptor contrasts. To convert the adaptor contrasts into “real-image-equivalent” afterimage contrasts, a power function of the form $C_a = bC_m^n$ was fitted to the mean settings, where C_a is adaptor contrast, C_m the matched contrast and b and n free parameters. There is no offset term in the power function, since it was not possible to measure sub-threshold afterimages. However by extrapolation of the fitted power function we were able to use adaptor contrasts that produced sub-threshold afterimages. The same procedure was employed with the achromatic stimuli, with real dark grey images being matched to dark grey afterimages. The power function parameters b and n are given for each observer and condition in Table A2, together with the goodness-of-fit measure R^2 (coefficient of determination).

Step 5: Detection thresholds with afterimage pedestals

The stimulus presentation protocol for the main, afterimage pedestal experiment is illustrated in Fig. 2a. The subject viewed two black rings on either side of the fixation point. On each trial the adaptor was first presented in both rings for 1000ms with a raised cosine temporal envelope. The adaptor onset was signalled by the fixation spot turning green. This was followed by the test stimulus presented within one of the two rings, linearly declining in contrast from its specified starting point to zero over 1500ms. The rate of decline was chosen to approximately match that of the perceived decline of the afterimage. The task for the subject was to decide which ring, left or right, contained the test. Trials were self-paced with each trial initiated by the key press of the previous response. A 3-up-1-down staircase was employed with a step fraction of 2.5 for the first 9 trials and 1.3 thereafter. The initial contrast was set to approximately double the threshold as determined by pilot studies. Feedback for an incorrect response was given by the fixation spot turning red. The session was terminated after 8 reversals. Subjects performed between 4 and 8 sessions per condition. For this experiment we term the dependent variable a “detection” rather than “discrimination” threshold because there was no *physical* pedestal present.

Table A3 gives the set of adaptor contrasts and real image pedestal contrasts used in the experiments. They were geometrically spaced and spanned most of the available range of the monitor.

Step 6: Detection thresholds with real image pedestals

The protocol for the real image pedestal experiment is illustrated in Fig. 2b. It paralleled the protocol used with the afterimage pedestals as closely as possible but without the adaptor and with the afterimage replaced by a real image pedestal. On each trial a pedestal was presented in both rings but the test increment added to just one, the task being to indicate the ring containing the test. One difference from the afterimage protocol is that the fixation circle filled with green at the onset of the pedestal-plus-test rather than at the onset of the adaptor. In this experiment the dependent variable is strictly speaking a “discrimination” not “detection” threshold, as the pedestal, unlike in the afterimage experiment, is physically present. However for ease of exposition we will use the term “detection threshold” for the real as well as for the afterimage pedestal data.

Psychometric function fitting

For each adaptor and pedestal contrast condition the number of correct detections were obtained for each test contrast. The data were then binned into 7 logarithmically-spaced test contrasts, and a log-Quick function fitted to the proportion correct responses as a function of mean within-bin log contrast, using a maximum-likelihood criterion, with thresholds estimated at the 75% correct level. Bootstrap errors on the fitted thresholds were obtained and these are the error bars in all graphs. Fitting routines were taken from the Palamedes toolbox (Prins & Kingdom, 2018).

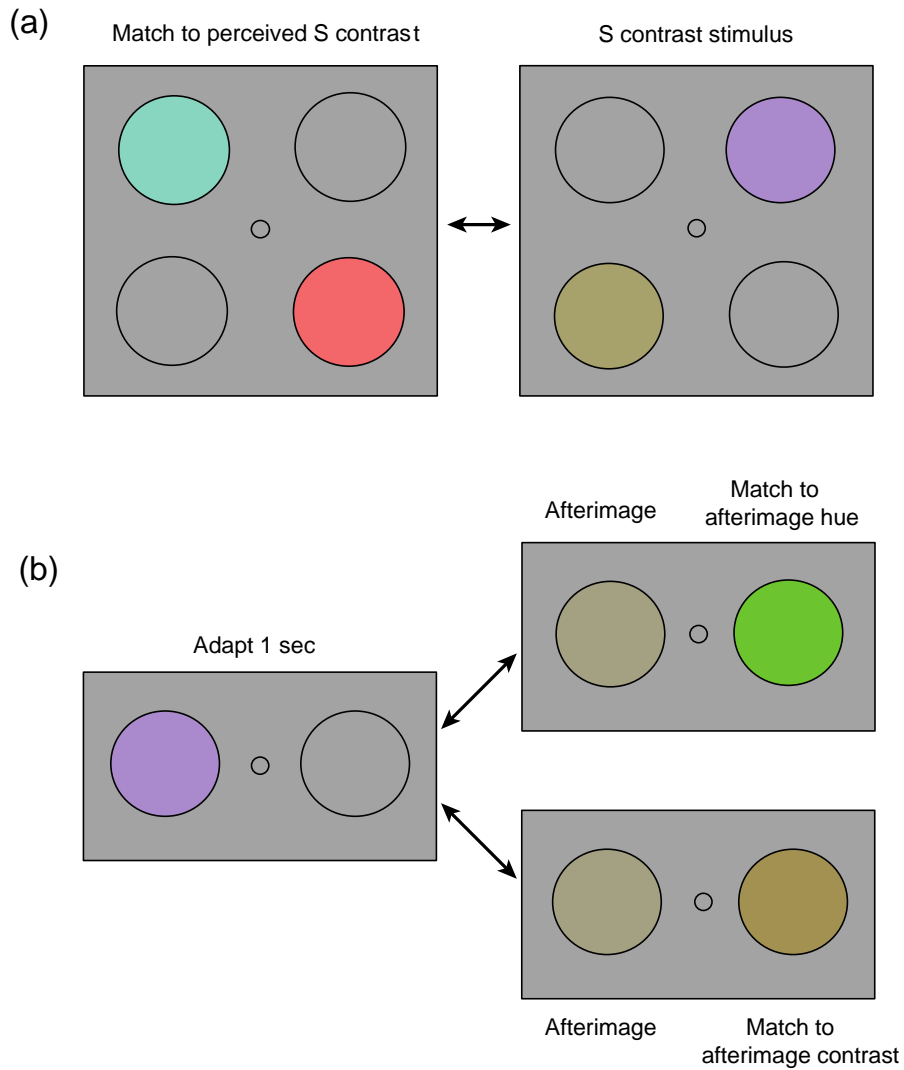


Figure 1. Protocols for (a) cardinal axis red-cyan versus violet-lime contrast matching, and (b) adjusting the hue and contrast of a real image to match that of the lime afterimage produced by a violet adaptor. See text for further details.

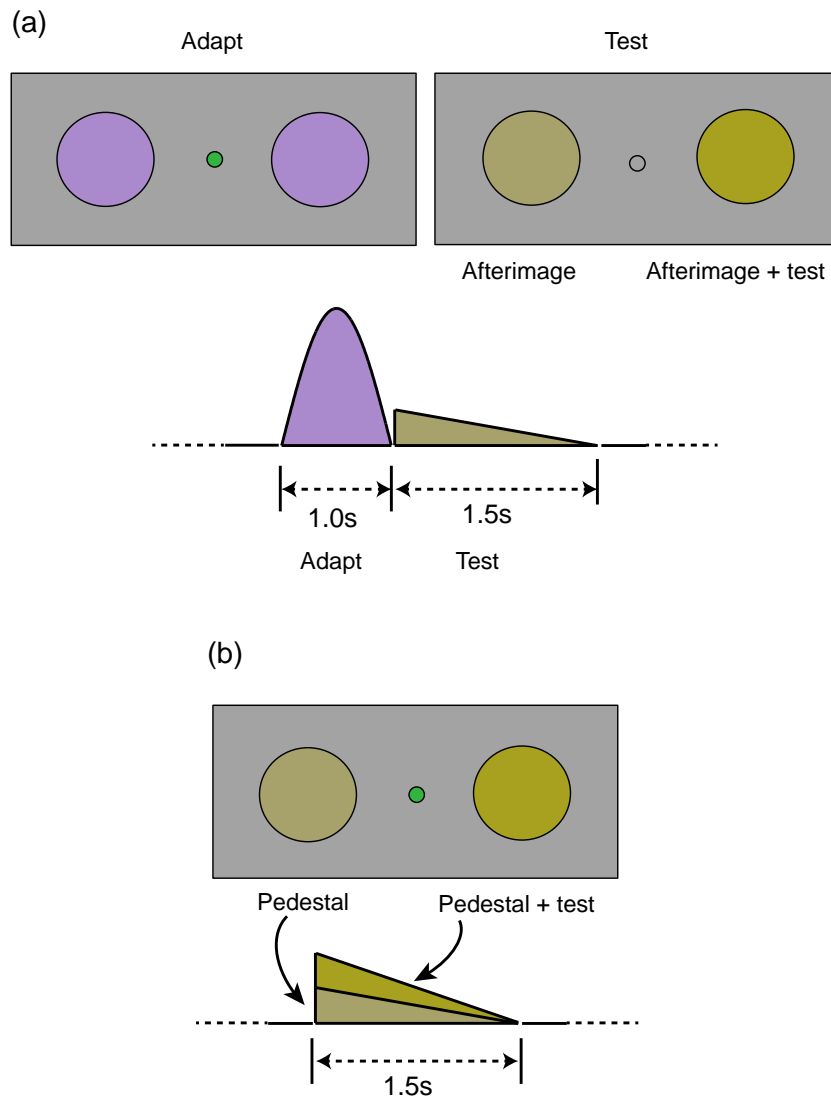


Figure 2. Protocol for main experiment applied to (a) a violet-induced lime afterimage and (b) a real lime image. See text for further details.

Results

Figs. 3 & 4 show respectively TvC functions for the chromatic and achromatic conditions. The units on both axes of the graphs have been normalized to the detection threshold of the test stimulus, i.e. in the absence of a pedestal, for both afterimage and real image pedestal conditions. The abscissae give the pedestal contrasts of the real images and the equivalent contrasts of the afterimages. As can be seen the range of equivalent afterimage pedestal contrasts is relatively small, reflecting the fact that afterimages are generally weaker than the real images that induce them.

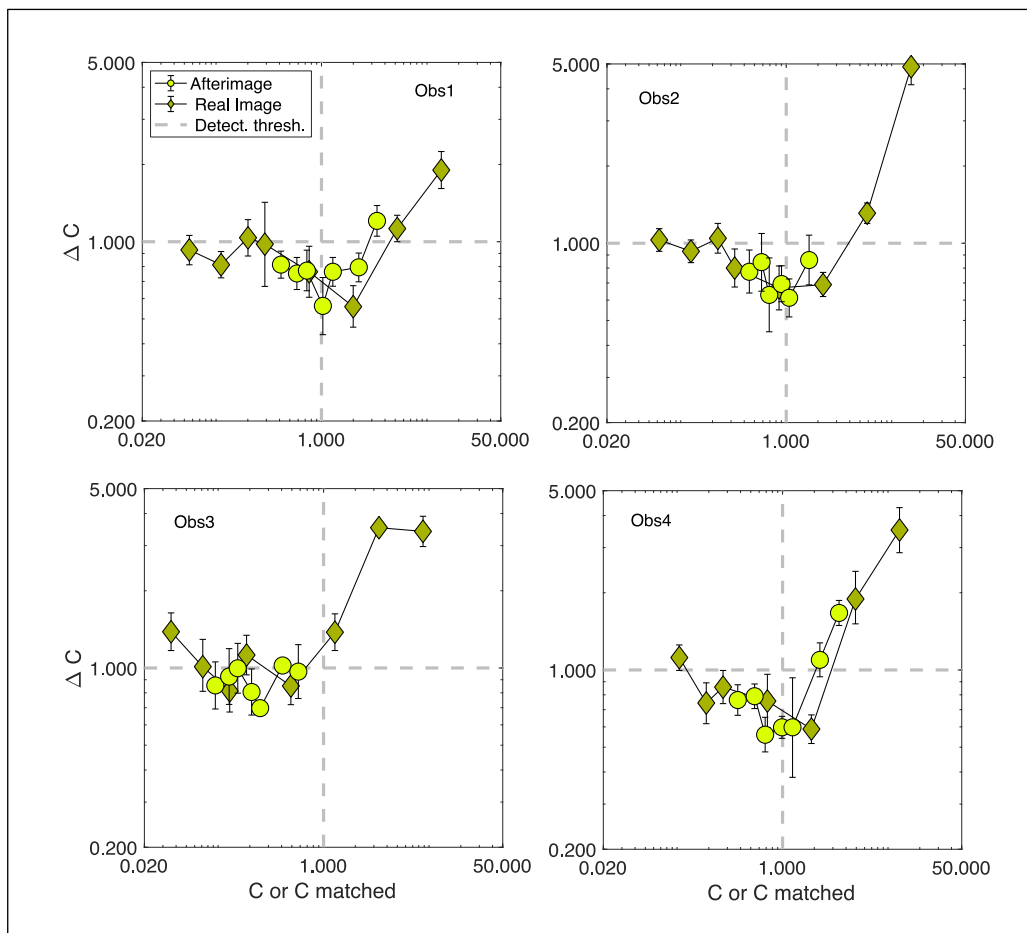


Figure 3. TvC functions for a lime test on a violet-induced lime afterimage pedestal (light lime filled circles) and for a real lime image pedestal (dark lime filled diamonds). The contrast of the afterimage is defined as the equivalent contrast of a matched real lime stimulus. Both axes are normalised to the detection threshold of the lime test.

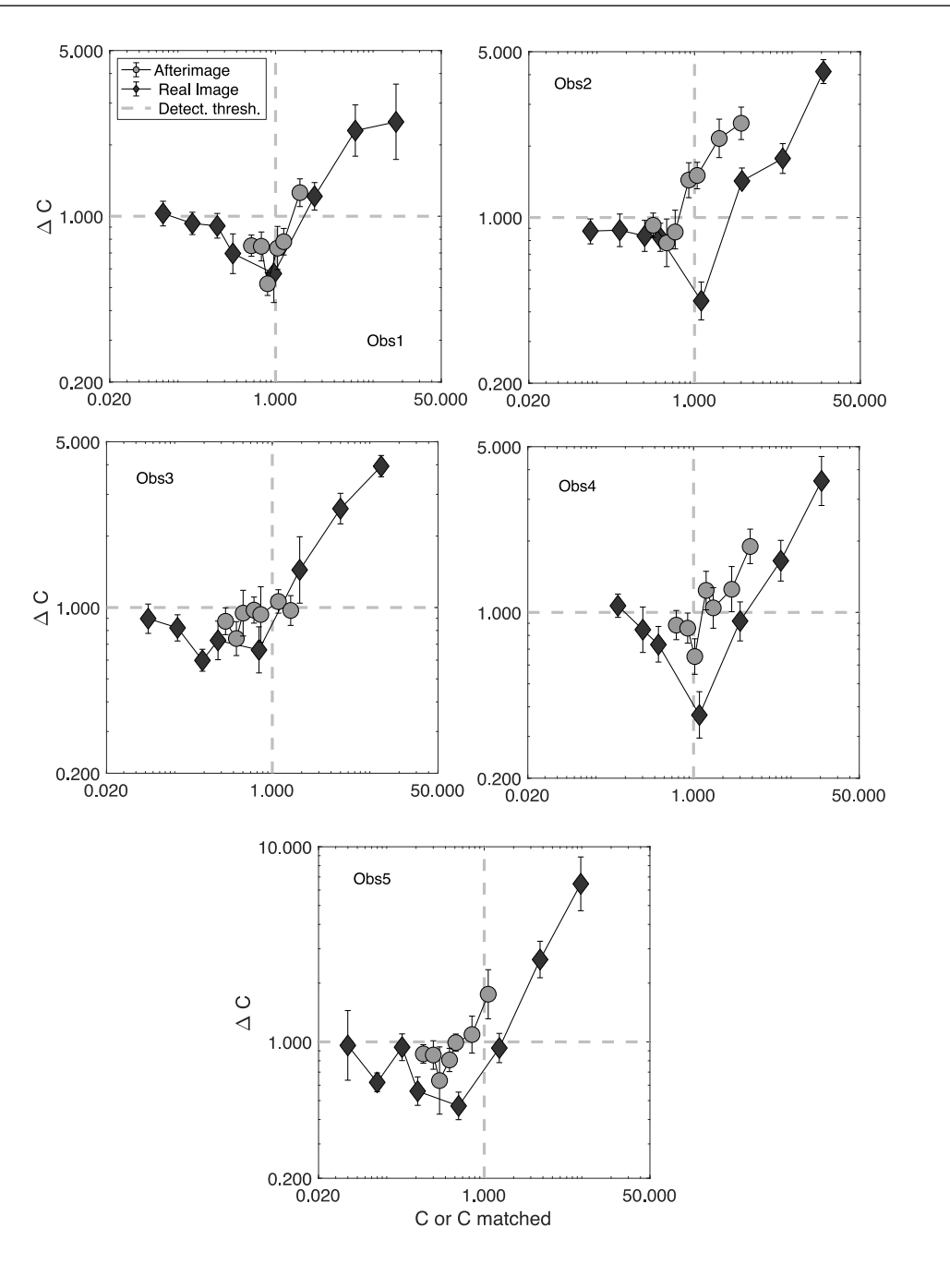


Figure 4. TvC functions for a dark-grey test on a white-induced dark-grey afterimage pedestal (light grey filled circles) and on a dark-grey real image pedestal (dark grey filled diamonds). The contrast of the afterimage is defined as the equivalent contrast of a matched real dark-grey stimulus. Both axes normalised to the detection threshold of the dark grey test.

The real-image pedestal data show in every case the classic dipper-followed-by-masking characteristic of contrast discrimination behaviour. With the afterimage data note first that many, and in a number of cases most of the afterimage pedestals fall to the left of the vertical grey lines, i.e.

within the sub-threshold pedestal region. A dipper is evident in most cases, but masking is only in some. Where masking is not evident the corresponding real image TvC function suggests that the switch from facilitation to masking takes place at contrasts higher than that achievable from the afterimage pedestals.

What is the magnitude of facilitation produced by the afterimage compared to real-image pedestals? To model the facilitation we employed the well-known contrast transduction model originally put forward by Legge & Foley (1980):

$$R(C) = \frac{C^p}{z+C^q} \quad \text{Eq. 2}$$

where R is the internal response to contrast C and p , q , and z are constants that determine the shape of the contrast response function. With suitable values of p , q , and z , R first accelerates then decelerates with C , resulting in the dipper-followed-by-masking pattern typical of contrast discrimination behaviour.

We incorporated Eq. 2 within a signal-detection-theory model that enabled us to utilize the full psychometric function with every threshold value (e.g. see Morgan, Chubb & Solomon, 2008; Baldwin, Baker & Hess, 2019). The signal-detection-theory measure d' can be computed thus:

$$d' = \frac{R(C + \Delta C) - R(C)}{\sigma} \quad \text{Eq. 3}$$

where C is pedestal contrast, ΔC is the test contrast increment and σ the standard deviation of internal noise. For the 2AFC task used here d' can be converted to proportion correct pC using the formula:

$$pC = \Phi \left[\frac{d'}{\sqrt{2}} \right] \quad \text{Eq. 4}$$

where Φ is the cumulative normal. Using a maximum likelihood criterion implemented by the Palamedes simplex-based routine PAL_minsearch and the signal-detection-theory routine PAL_SDT_2AFC_DPtoPC, we obtained values of p , q , z and σ that best fitted the full set of psychometric functions for each set of data.

Following the suggestion of an anonymous reviewer we also fitted a straight-line model to the full psychometric function data, in order to determine whether this produced a better fit. This

was a distinct possibility for those conditions in which the thresholds varied little with pedestal contrast. To model the data with a straight line we used the following signal-detection-theory model:

$$d' = (g\Delta C)^\tau \quad \text{Eq. 5}$$

where the two free parameters are gain g and transducer exponent τ . When combined with Eq. 4 to convert the d' s to proportion correct, the full set of psychometric functions for each plot were fitted with Eq. 5 to estimate a single value of g and τ and the straight line through the data calculated as before for a d' of 1, given this time by $1/g$.

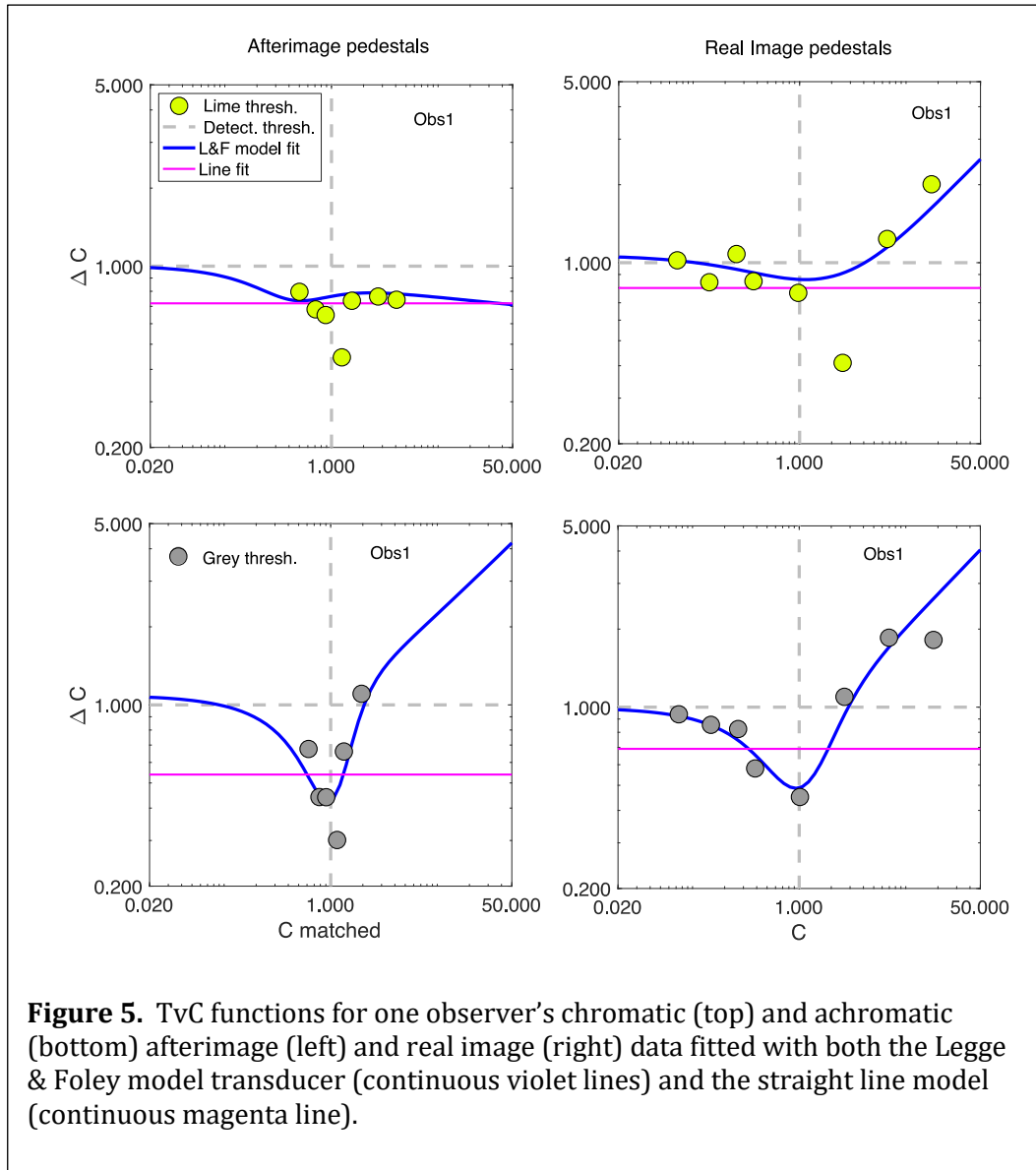
To compare the two model threshold curves with the data thresholds we recalculated the data thresholds with the signal-detection model given in Eqs. 4 and 5, this time fitted separately to each psychometric function. To do this we used the Palamedes routines PAL_SDT_PFML_Fit and PAL_SDT_2AFC_DPtoPC. As with the straight-line fit the threshold was calculated for a d' of 1, given by $1/g$.

The resulting model fits are shown for just one (naïve) observer's data in Fig. 5 as the continuous blue lines for the Legge & Foley model, and the magenta lines for the straight-line model. To compare the fit of the two models we computed Akaike's Information Criterion (AIC) for each model, which takes into account the number of free parameters: four for the Legge & Foley model and two for the straight-line model. The advantage of fitting the models to the whole set of psychometric functions per condition is that because a large number of samples (over 1000) is used in the fit one does not need to incorporate the correction for low samples in the AIC formulation (Cavanaugh, 1997), which would be necessary if the fit was applied to the threshold-alone data. The fitted parameters of both models are given in Table A4, along with AIC values. The difference in AIC values between the Legge & Foley and straight-line model is shown in the last column, with a negative value implying a better fit for the Legge & Foley model.

To estimate the magnitude of facilitation from the Legge & Foley model fitted function we calculated the percentage reduction in thresholds from the zero pedestal ΔC to the minimum ΔC , which we term the "dip %", and this is also provided in Table A4.

Finally we repeated the chromatic experiment on two observers using a red rather than lime target, and the results are shown in Fig. 6, along with the lime target results. The abscissa values were normalised in the same way as in the main experiment, i.e. normalised to the lime target thresholds, as the pedestal color, lime, was the same for both target colors. The ordinate values were

normalised to the respective lime and red target thresholds. The red color was at the positive end of the $L-M$ axis, which is orthogonal to the S cone axis from which the adaptor and test in the main experiment were taken. As Fig. 6 shows the results for the red target differ somewhat between the two observers, but in neither observer is there evidence that thresholds for the red target were reduced in the subthreshold region, either for the afterimage or real-image pedestals.



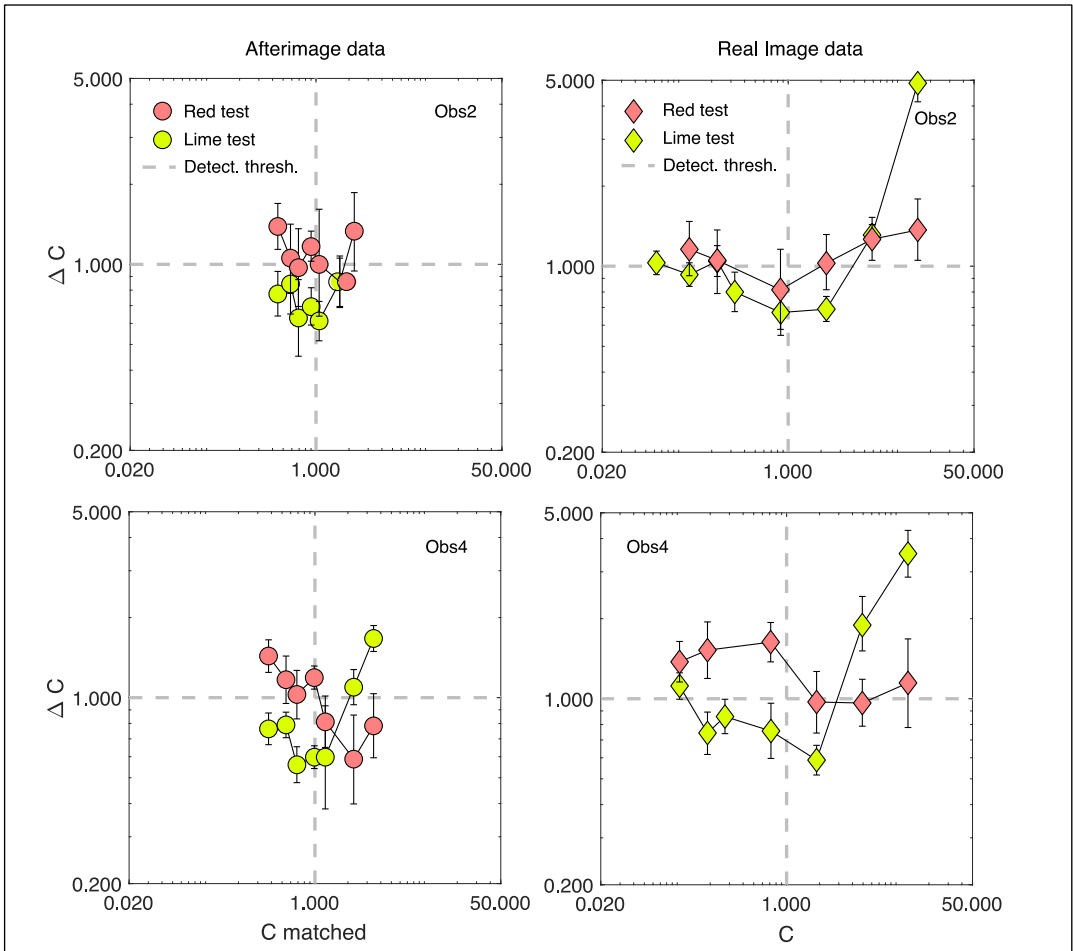


Figure 6. TvC functions for a lime (filled lime) and red (filled red) test on a violet-induced lime afterimage pedestal (circles) and on a real lime image pedestal (diamonds). The afterimage pedestal contrasts are defined as equivalent contrasts of a matched real lime stimulus, normalised to the detection threshold of a lime stimulus. The ordinate values are normalised to the thresholds for the lime and red tests.

Discussion

In most cases the Legge & Foley model gave a better fit than the straight-line model for the afterimage data (and in all cases for the real image data). In the two cases where it did not, Observer 1's color afterimage (see Fig. 6) and Observer 3's achromatic afterimage data, it is clear nevertheless that there is facilitation, as evidenced by the fact that with the position of the straight-line fit along the vertical, which indicates the average of the fitted threshold values, falls below that of the grey dashed line indicating the zero-pedestal threshold. The mean values for the reduction in thresholds from the zero pedestal to minimum threshold estimated from the Legge & Foley model - the values of dip % in Table A4 - were 39% and 26% for respectively the chromatic and achromatic afterimage pedestals, and 30% and 48% for the corresponding real image pedestals. However when using the same violet adaptor and lime afterimage but this time with a red rather than lime real-image test, there was no evidence of facilitation, at least in the subthreshold pedestal region. The facilitation found here for afterimage pedestals acting on real image tests supports the idea that afterimages can be represented at sub-threshold levels and at the point where real and afterimage stimuli are combined in the cortex to mediate contrast discrimination.

There are two obvious limitations of the present study. The first lies in the temporal characteristics of the test stimuli. Whereas the temporal profiles of the real image pedestals and real-image tests were identical (see Fig. 2b), the same cannot be said for the temporal profiles of the afterimage pedestals and real-image tests. Although the temporal profiles of the real image tests - a step function followed by linear decline over 1.5 secs - were designed to be as similar as possible to those of the perceived temporal profiles of the afterimages, they were based on casual observation and therefore inevitably not optimal. As a result the set of temporal channels signaling the afterimages will not be quite the same as those detecting the real images. The senior author for example perceived a sharp temporal transient at the onset of the achromatic real image (it was after all a step function) that he did not always perceive in the afterimage, possibly the reason why the facilitation from the achromatic afterimage pedestals was much less than from the achromatic real image pedestals (on average 26% compared to 48%). No such sharp transients were perceived in either the chromatic real images or chromatic afterimages, and it is notable that in this case the facilitation was on average greater from the afterimage pedestals (on average 39% compared to 30%).

The second limitation lies in the method of equating the afterimage and real pedestal contrasts. We used a matching protocol in which the perceived contrasts of the afterimages

produced by various adaptor contrasts were matched to those of real images, then fitting power functions to the data in order to convert the adaptor contrasts into real-image-equivalent afterimage contrasts. However the matches were only possible when the afterimages were visible, i.e. suprathreshold, so for sub-threshold afterimages the equivalent contrasts were only extrapolations of the power function fits, and thus likely inaccurate. This is likely the reason for the especially poor matches between the real and afterimage pedestal data in the achromatic conditions shown in Fig. 4.

Model of the afterimage pedestal and test

Zaidi et al.'s (2012) study provides strong evidence that both the adaptation preceding an afterimage as well as the afterimage itself likely originates in retinal ganglion cells (RGCs). They recorded responses of macaque RGCs to stimuli modulated along each pole of a cardinal axis (e.g. red-grey, violet-grey, lime-grey). While each cell responded to both poles of its preferred cardinal axis, with one pole enhancing and the other suppressing the response, it was the rebound in the cell's response when the stimulus turned grey that mirrored the psychophysical observations of afterimages obtained under similar spatio-temporal conditions.

In relation to the present study, in which TvC functions were measured, the RGC explanation for afterimages provided by Zaidi et al. needs to be squared with the psychophysical evidence for separability of the poles of the cardinal axes at the point of stimulus detection: McLellan & Eskew (2000) for the S-cone axis, Huang, Kingdom & Hess (2006) for the luminance axis, and Sankeralli and Mullen (2001) for all three cardinal axes. Such separability is presumably a consequence of the half-wave-rectification of RGC outputs at post-retinal sites, such as the LGN and cortex.

Figure 7 shows a putative scheme to account for our findings that is in keeping with both Zaidi et al. as well as post-retinal half-wave-rectification. In the figure a "blue-OFF/yellow-ON" RGC produces a positive rebound response after the offset of the violet adaptor in both 2AFC alternatives. In one of the rebounds the response to the lime test is added, and both rebounds are preserved following half-wave-rectification at a post-retinal site, allowing their comparison to be made at the cortical decision stage.

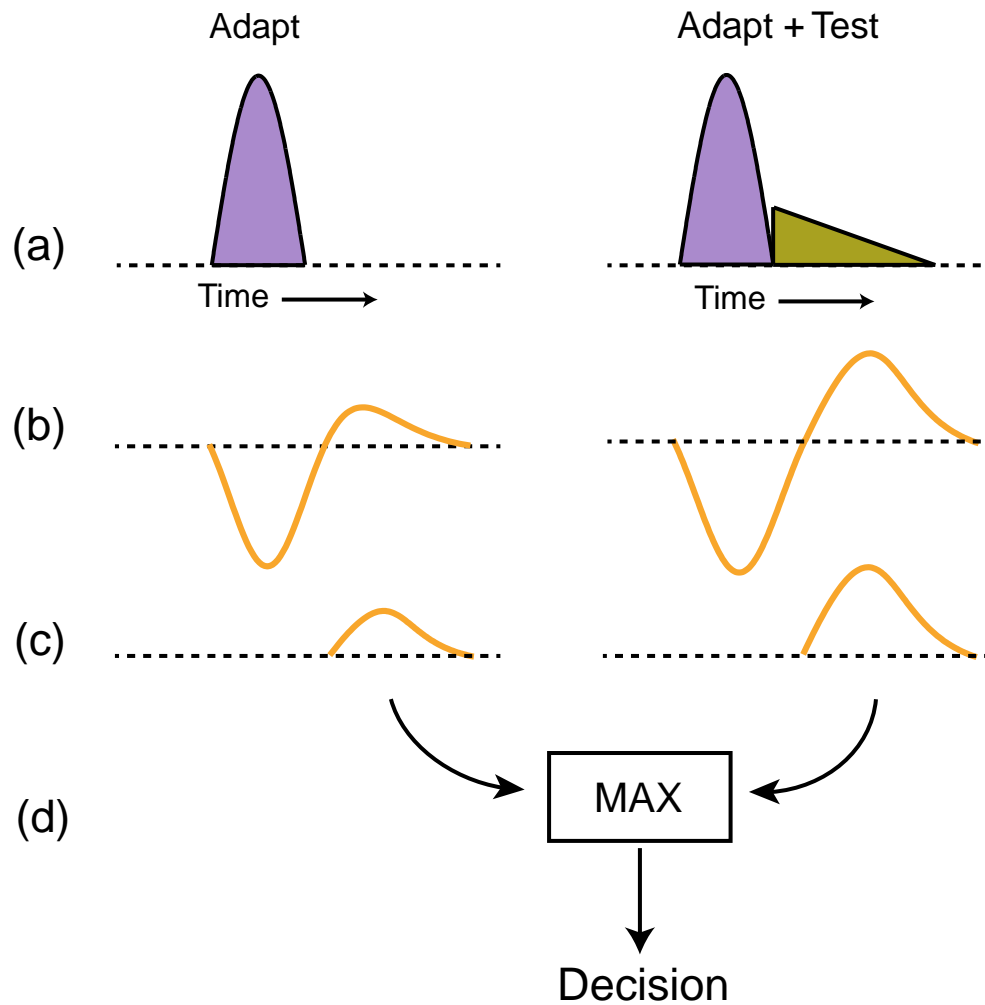


Figure 7. Schematic of how an afterimage acts as a pedestal in a TvC task. (a) temporal arrangements of the violet adaptors and lime test forced-choice pair. (b) hypothetical responses of a “blue-OFF/yellow-ON” retinal ganglion cell; note the positive rebounds in both responses after the offset of the adaptor and the added response to the lime test in one of the rebounds. (c) half-wave-rectification of the responses in the LGN/cortex, preserving the afterimage and test signals. (d) cortical decision stage where the maximum (MAX) of the two responses is selected as the one containing the test.

What of test colors opposite to the pole of the lime afterimage and of afterimages generated along the red-cyan axis?

One might suppose that it would have been useful to test the condition in which the test was opposite in color to that of the lime afterimage, i.e. the same color as the adaptor - violet. We tried this but soon realized that the task was too problematic to produce sensible data. Consider the appearance of a violet test added to a lime afterimage as the test is gradually reduced in contrast from its starting point at the beginning of the staircase. At high contrast the test appears violet, then at some intermediate contrast it cancels with the lime afterimage to produce grey, then at very low contrasts appears lime. The comparison afterimage without the added test on the other hand appears lime throughout. Thus the observer is confronted with categorical changes in the appearance of the test image with no such categorical changes in the appearance of the comparison image, making it virtually impossible to determine on any given trial the basis for making a correct decision. Hence we did not collect data for this condition.

With regard to afterimages generated along the red-cyan, or intermediate axes of the DKL color space, while we predict that the results would be similar to the ones found here, this will have to be confirmed by future studies.

Relation to surround-induced color studies

The results of this study using afterimages parallel those of studies in which the colors of test regions are induced by surround colors. For example Livitz et al. (2016) showed that the hues of afterimage and surround-induced colors were the same if elicited by same-color adaptors and inducers. More directly parallel to the present study, McCourt & Kingdom (1996) measured detection thresholds for sinusoidal luminance gratings in the “grating induction” stimulus, in which an illusory grating is observed in a uniform stripe that runs orthogonal to the bars of a real, inducer luminance grating. In this case the illusory grating served as a pedestal with an apparent contrast determined by the contrast of the inducer grating, with the tests real gratings added in-phase with the apparent modulations of the induced gratings. McCourt & Kingdom found that the illusory grating pedestals produced dipper functions in test thresholds comparable to those of real grating pedestals matched in apparent contrast. They interpreted their findings as consistent with the idea that the same mechanism signaled real and illusory gratings. More recently Maertens and Wichmann (2013) and Maertens, Wichmann, and Shapley (2015) considered whether luminance

test thresholds were affected by luminance pedestals perceived to lie either inside or outside of a simulated shadow, which strongly affected their lightness. They found that provided the test and pedestal had the same spatial configuration, test thresholds differed significantly between the two configurations, in keeping with the idea that the pedestal lightnesses were encoded by a common mechanism.

Acknowledgements

This work was funded by the Canadian Institute of Health Research grant #MOP 123349 awarded to F.K.

References

- Abbonizio, G., Langley, K. & Clifford, C. W. G. (2002) Contrast adaptation may enhance contrast discrimination. *Spatial Vision*, 16(1):45-48.
- Anstis, S., Rogers, B., & Henry, J. (1978). Interactions between simultaneous contrast and colored afterimages. *Vision Research*, 18, 899–911.
- Anstis, S., Vergeer, M., & Van Lier, R. (2012). Luminance contours can gate afterimage colors and “real” colors. *Journal of Vision*, 12 (10):2, 1–13.
- Brainard, D. H. & Stockman, A. (2010). Colorimetry. In *Handbook of Optics: Volume III - Vision and Vision Optics, Third Edition* (Ed. Michael Bass). The McGraw-Hill Companies, Inc.
- Baldwin, A. S., Baker, D. H. & Hess, R. F. (2016) What Do Contrast Threshold Equivalent Noise Studies Actually Measure? Noise vs. Nonlinearity in Different Masking Paradigms. *PLoS ONE* 11(3): e0150942.
- Cavanaugh, J. E. (1997), Unifying the derivations of the Akaike and corrected Akaike information criteria, *Statistics & Probability Letters*, 31 (2): 201–208.
- Cole, G.R., Hine, T. & McIlhagga, W. (1993) Detection mechanisms in L-, M-, and S-cone contrast space. *Journal of the Optical Society of America A, Optics, Image Science, and Vision*, 10, 38-51.
- Derrington, A. M., Krauskopf, J., & Lennie, P. (1984). Chromatic mechanisms in lateral geniculate nucleus. *J. Physiol.*, 241–265.

- Dong, B., Holm, L. & Bao, M. (2017). Cortical mechanisms for afterimage formation: evidence from interocular grouping. *Scientific Reports*, 7, 41101.
- Eskew, R. T., McLellan, J. S., & Giulianini, F. (1999). Chromatic detection and discrimination. In K. Gegenfurtner & L. T. Sharpe (Eds.), *Color vision: From molecular genetics to perception* (pp. 345–368). Cambridge: Cambridge University Press.
- Feitosa-Santana, C., D'Antona, A. D., & Shevell, S. K. (2011). What kinds of contours bound the reach of filled-in color? *Journal of Vision*, 11(2):2, 1–11.
- Greenlee, M. W. & Heitger, F. (1988). The functional role of contrast adaptation. *Vision Research*, 28, 791-797.
- Hering, E. (1874/1964). *Outlines of a theory of the light sense*. (L.M.H.D. Jameson, Trans.). Cambridge, MA: Harvard University Press.
- Huang, P.-C., Kingdom, F. A. A., & Hess, R. F. (2006). Only two phase mechanisms, \pm cosine, in human vision. *Vision Research*, 46, 2069–2081.
- Kelly, D. H. & Martinez-Uriegas (1993). Measurements of chromatic and achromatic afterimages. *J. Opt. Soc. Amer. A.*, 10(1):29-37.
- Kingdom, F. A. A., Rangwala, S. & Hammamji, K. (2005) Chromatic properties of the Colour shading Effect. *Vision Research*, 45, 1425-1437.
- Krauskopf, J., Williams, D.R. & Heeley, D.W. (1982). Cardinal directions in cardinal space. *Vision Research*, 22, 1123–1131.
- Legge, G. E., & Foley, J. M. (1980). Contrast masking in human vision. *Journal of the Optical Society of America*, 70, 1458–1471.
- Livitz, G., Riesen, G., Mingolla, E., & Eskew, R., (2015) Canceling a hue of a negative afterimage in solid and perceptually-filled color images. *Journal of Vision*, 15, 402-402.
- Livitz, G., Riesen, G., Shepherd, T., Mingolla, E., & Eskew, R., (2016). Afterimages and induced colors have the same hue: Implications for discounting illuminants. *Journal of Vision*, 16, 1145-1145.
- Maertens, M., & Wichmann, F. A. (2013). When luminance increment thresholds depend on

- apparent lightness. *Journal of Vision*, 13(6), 21. 1–11.
- Maertens, M., Wichmann, F. A., & Shapley, R. M. (2015). Context affects lightness at the level of surfaces. *Journal of Vision*, 15(1), 15. 1–15.
- McCourt, M. E. & Kingdom, F. A. A. (1996). Facilitation of luminance grating detection by induced gratings. *Vision Research*, 36, 2563-2573.
- McLellan, J.S. & Eskew, R.T. (2000). ON and OFF S-cone pathways have different long-wave cone inputs. *Vision Research*, 40, 2449–2465.
- Morgan, M, Chubb, C & Solomon, J. A. (2008) A 'dipper' function for texture discrimination based on orientation variance. *Journal of Vision*, 8(11)(9):1–8.
- Powell, G., Bompas, A., & Sumner, P. (2012). Making the incredible credible: Afterimages are modulated by contextual edges more than real stimuli. *Journal of Vision*, 12 (10):17, 1-13.
- Prins, N. & Kingdom, F. A. A. (2018). Applying the model-comparison approach to test specific research hypotheses in psychophysical research using the Palamedes toolbox. *Frontiers in Psychology*, 9:1250.
- Ripamonti, C., Woo, W. L., Crowther, E. & Stockman, A. (2009). The S-cone contribution to luminance depends on the M- and L-cone adaptation levels: Silent surrounds? *Journal of Vision*, 9:3(10), 1-16.
- Ross, J. & Speed, H. D. (1991). Contrast adaptation and contrast masking in human vision. *Proc. R. Soc. Lond. B.*, 246, 61-69.
- Ross, J., Speed, H. D. & Morgan, M. J. (1993). The effects of adaptation and masking on incremental thresholds for contrast. *Vision Research*, 33, 2051-2056.
- Sankeralli, M. J. & Mullen, K. T. (1996) Estimation of the L-, M-, and S-cone weights of the postreceptoral detection mechanisms. *J. Opt. Soc. Am. A* 14, 2633-2646.
- Sankeralli, M.J. & Mullen, K.T. (2001). Bipolar or rectified chromatic detection mechanisms? *Visual Neuroscience*, 18, 127-135.
- Schwartz, O., Hsu, A. & Dayan, P. (2007). Space and time in visual context. *Nature Reviews Neuroscience*, 8, 522-535.
- Solomon, J. A. (2009). The history of dipper functions. *Attention, Perception, & Psychophysics*, 71(3), pp. 435-443.
- Smith, V. C. & Pokorny, J. (1975) Spectral sensitivity of the foveal cone photopigments between 400 and 700 nm. *Vision Research*, 15, 161-171.
- Stromeyer, C. F III, Cole, G. R. & Kronauer, R. E. (1985). Second-site adaptation in the red-green

- chromatic pathways. *Vision Research*, 25, 219-237.
- Suzuki, S. & Grabowecky M. (2003). Attention during adaptation weakens negative afterimages. *J Exp. Psychol. Hum. Percept. Perform.* 29(4):793-807.
- Van Lier, R., Vergeer, M., & Anstis, S. (2009). Filling in afterimage colors between the lines. *Current Biology*, 19, R323–R324.
- Webster, M. A. (1996). Human color perception and its adaptation. *Network: Computation in Neural Systems*, 7, 587-634.
- Zaidi, Q., Ennis, R., Cao, D. & Lee, B. (2012). Neural locus of color afterimages. *Current Biology*, 22(3):220-224.

Appendix

Table A1

Obs.	Isolum. $LUM/(L-M)$ ratio	Isolum. LUM/S ratio	Cardinal axis $S/(L-M)$ contrast ratio	Lime afterimage perceived color direction (deg)
1	-0.124	-0.016	1.684	181
2	-0.0272	0.001	1.728	180
3	-0.222	0.007	2.525	180
4	-0.413	0.045	5.49	184

Table A2

Obs.	Lime afterimage equiv. cont. params.			Dark-grey afterimage equiv. cont. params		
	b	n	R^2	b	n	R^2
1	0.117	0.589	0.94	0.0663	0.397	0.91
2	0.0524	0.453	0.92	0.0465	0.54	0.95
3	0.0536	0.589	0.29	0.0615	0.433	0.98
4	0.159	0.621	0.98	0.0653	0.453	0.99
5				0.0663	0.399	0.87

Table A3

Violet adaptor contrasts	0.0	0.0171	0.0309	0.0447	0.0809	0.117	0.3059	0.6	
Real Lime pedestal contrasts	0.0	0.0013	0.0025	0.0045	0.0065	0.0171	0.0447	0.117	0.3059
Bright adaptor contrast	0.0	0.0171	0.0309	0.0447	0.0809	0.117	0.3059	0.8	
Real Dark-grey pedestal contrasts	0.0	0.0013	0.0025	0.0045	0.0065	0.0171	0.0447	0.117	0.3059

Table A4

Condition	Obs.	Legge&Foley fit						Straight-line fit			
		p	q	z	s	AIC	dip %	T	τ	AIC	Δ AIC
Lime after-image	1	3.45	2.44	0.156	0.873	1579	30	0.72	0.83	1572	7
	2	2.11	2.09	6.38	0.195	1229	42	0.55	0.49	1231	-2
	3	3.10	2.98	1.18	0.56	1820	33	0.83	0.41	1831	-11
	4	2.88	2.41	2.91	0.43	1282	49	0.71	0.57	1307	-25
Lime real image	1	1.50	0.91	2.42	0.317	977	19	0.80	0.55	992	-15
	2	1.59	1.46	13.7	0.084	939	42	0.74	0.41	1011	-72
	3	3.03	2.48	0.75	0.71	943	30	1.1	0.47	989	-46
	4	1.70	1.35	4.48	0.24	1104	29	0.84	0.42	1155	-51
Dark-grey after-image	1	4.50	3.91	1.51	0.50	1323	61	0.53	0.68	1364	-41
	2	3.81	3.28	0.57	0.66	1446	40	0.86	0.48	1507	-61
	3	1.07	1.66	38.9	0.028	1857	0	0.95	0.61	1838	19
	4	2.07	1.64	1.54	0.40	1468	28	0.97	0.80	1506	-38
	5	*	*	*	*	*	0	0.61	0.52	1696	*
Dark-grey real image	1	3.03	2.47	1.48	0.4	889	51	0.69	0.49	942	-53
	2	2.18	1.56	0.91	0.50	1994	26	0.63	0.37	2065	-71
	3	2.92	2.39	0.73	0.49	949	39	0.70	0.41	1011	-62
	4	2.99	2.47	2.77	0.37	1668	56	0.86	0.36	1770	-102
	5	10.4	9.9	0.043	0.66	2058	68	0.41	0.25	2129	-71

Note: * unable to produce a reliable fit